LA-UR-16-28348
Approved for public release; distribution is unlimited.

Title: Continuous Energy Photon Transport Implementation in MCATK

Author(s): Adams, Terry R.
Trahan, Travis John
Sweezy, Jeremy Ed
Nolen, Steven Douglas
Hughes, Henry Grady III
Pritchett-Sheats, Lori A.
Werner, Christopher John

Intended for: Report

Issued: 2016-10-31

Continuous Energy Photon Transport Implementation in MCATK

The MCATK Team,

Terry Adams[a], Travis Trahan[a], Jeremy Sweezy[a], Steve Nolen[a],
H. Grady Hughes[a], Lori Pritchett-Sheats[b], and Chris Werner[a]

[a]*Monte Carlo Methods, Codes, and Applications Group (XCP-3); X-Computational Physics Division*
[b]*Computational Physics and Methods Group (CCS-2); Computer, Computational, and Statistical Sciences Division*
P.O. Box 1663, Los Alamos National Laboratory, Los Alamos, New Mexico 87545 USA
26 October 2016, version 1.0

Abstract

The Monte Carlo Application ToolKit (MCATK) code development team has implemented Monte Carlo photon transport into the MCATK software suite. The current particle transport capabilities in MCATK, which process the tracking and collision physics, have been extended to enable tracking of photons using the same continuous energy approximation. We describe the four photoatomic processes implemented, which are coherent scattering, incoherent scattering, pair-production, and photoelectric absorption. The accompanying background, implementation, and verification of these processes will be presented.

Keywords: Monte Carlo, photon transport, coherent scattering, incoherent scattering, pair-production, photoelectric effect, photon production, MCATK

Email address: mcatk@lanl.gov (The MCATK Team)

Contents

List of Figures

List of Tables

1. Introduction

The Monte Carlo Application ToolKit (MCATK) (Adams et al., 2015; Sweezy et al., 2015) is a modern Monte Carlo particle transport parallel-aware software library developed at Los Alamos National Laboratory. It is designed to provide new component-based functionality for existing software as well as provide the building blocks for specialized applications. The purpose of this paper is to explain the methodology that MCATK employs for continuous energy photon transport, including a description of the relevant central physics processes, implementations, potential pitfalls, and future improvements.

We leverage the basic particle transport kernels for neutron tracking and collisions presently in MCATK with the corresponding changes for continuous energy photon transport. In this report, our *focus* is on the basic description of the physics for four photoatomic processes (photons interacting with an atom) and the implementation of these processes: coherent scattering, incoherent scattering, pair-production, and photoelectric absorption. A good reference that describes the physics for these photoatomic interactions is Evans (1982). An overview of the Monte Carlo photon transport and sampling algorithms is found in Carter and Cashwell (1977) and Lux and Koblinger (1991).

Section 2, the report is broken into individual subsections covering each of the four photoatomic processes of interest: coherent scattering (Subsection 2.1), incoherent scattering (Subsection 2.2), pair-production (Subsection 2.3), and photoelectric effect (Subsection 2.4). A description of photons created from neutron interactions is given in Section 3. Verification results for the MCATK implementation are presented in Section 4. Section 5 summarizes this report.

2. Photoatomic Interactions

> *It is well known that electromagnetic radiation can be scattered by charged particles that are free to respond to the incident electromagnetic wave. In the quantum theory, this process must be described as the absorption of the quantum from the incident light, and the emission of another quantum in the new direction. Insofar as energy-momentum relations are concerned, however, this process can equally well be described as the scattering for a single particle, which is not destroyed, but which merely suffers a change of energy and momentum.*
>
> -*David Bohm* (Bohm, 1958, p. 33)

Often electromagnetic radiation is classified by the frequency (or the related wavelength) it possesses. A good example is the common electromagnetic spectrum chart, which starts at one end of the chart (the higher frequency spectrum) and decreases in frequency moving to the other end of the chart (e.g., gamma-rays, X-rays, ultra-violet, visible, infrared, and so on). Photons are nothing more than electromagnetic radiation. It is often more convenient to classify photons by their *mode* of origin. For example, gamma-rays accompany nuclear transitions; annihilation radiation is emitted by a positron and electron combining; continuous X-rays are produced by the acceleration of charged particles; and characteristic X-rays are emitted by the atomic transitions of bound electrons.

Regardless the mode of origin, the subsequent interactions depend only on the photon's quantum energy, $E = h\nu$, where h is Planck's constant and ν is the photon frequency (Einstein, 1905, 1967).

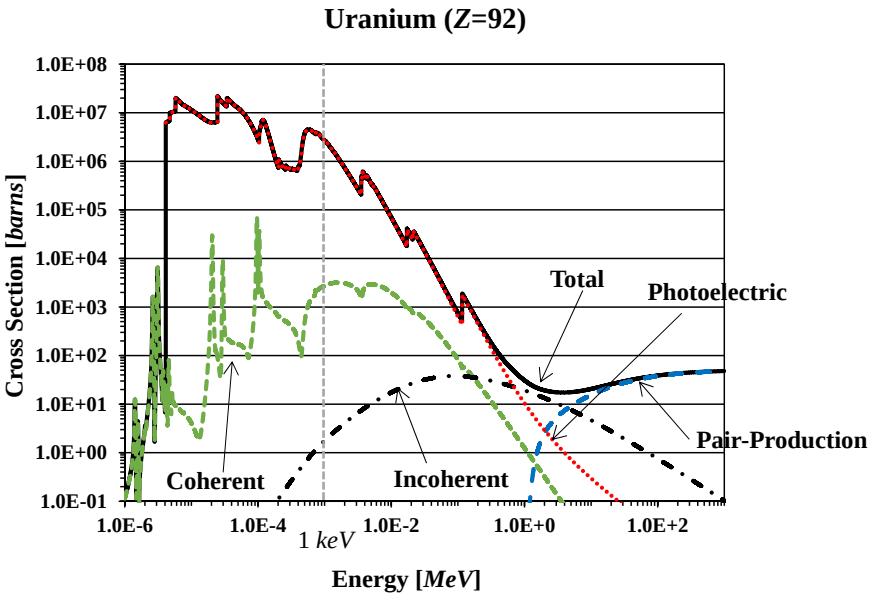

Figure 1: An example of the photoatomic interaction cross sections as a function of energy for the element Uranium. The four partial cross sections of each interaction and the total cross section are presented. The data plotted is from the `eprdata12` library. For previously released libraries like `mcplib04`, the data tables do not extend below 1 *keV* in energy as indicated by the vertical gray dashed line.

For instance, once a gamma-ray is emitted from a nucleus then its material interactions are that of an *individual photon* at a given energy. The photon, in single events, is either scattered or absorbed. For the interested reader, these and other interactions are described in Evans (1982), Hubbell (1999), Hubbell (2006b), and Pratt (2014).

Photons may interact with an atom as a whole, as with electrons bound to the nucleus, or they may interact with the nucleus itself. The former interactions are referred to as *photoatomic reactions*, while the latter are referred to as *photonuclear reactions* or *photodisintegration*. Photonuclear reactions typically have a high threshold (most at about 8 *MeV*), are dominated by photoatomic reactions for even higher energies (Evans, 1982, p. 673-674), and are a small component of the total photon cross section. For this reason, *only* photoatomic reactions are modeled by MCATK at this time.

The four photoatomic processes[1] to be presented in this report are coherent (elastic) scattering, incoherent (inelastic) scattering, pair-production (absorption), and photoelectric effect (absorption). Fig. 1 illustrates, for Uranium (atomic number, $Z = 92$), the four partial cross sections for each type of interaction and the total cross section which is the sum of the partials.[2]

Coherent scattering may happen when an incident photon interacts with an electron. The recoiling electron then accelerates before emitting radiation at the same frequency and phase as the

[1] Evans (1982, p.729) describes five interactions of photons with matter and categorizes them into primary, secondary, and tertiary processes and particles. Of the primary processes, four are photoatomic processes and the fifth process is the photonuclear reaction. We will be using Evan's categorizations in this report.

[2] Note that MCATK uses a default minimum photon energy cutoff of 1 *keV*.

incident photon (see Evans (1958, p. 291) and Evans (1982, p. 819)). It appears as if the photon has changed direction without changing energy and is *elastically* scattered. Coherent scattering, which is a primary photon process, occurs at lower energies and is typically dominated by the other three primary processes at all energies as seen by the cross sections in Fig. 1. Coherent scattering is forward peaked, particularly at high energies, and so its effect is often negligible for high-energy photons.

Incoherent scattering, like coherent scattering, occurs when an incident photon interacts with an electron. Unlike coherent scattering, the outgoing photon has a different frequency, and therefore a different energy, than the incident photon (Evans, 1982, p. 674). The outgoing photon can be thought of as a secondary photon. The expected total energy of the system is conserved due to an accompanying outgoing recoil electron (a secondary electron). But due to transfer of energy to the target electron from the incident photon then the scattering event can be thought of as *inelastic*. Fig. 1 shows that incoherent scattering is most significant at intermediate energies.

Pair-production occurs when a photon with energy at least twice that of the rest-mass of an electron (i.e., an energy greater than $\sim 1.022\ MeV$), interacts with the field of a nucleus to spontaneously produce an electron-positron pair (Evans, 1982, p. 701). The paired particles can be thought of as secondary electrons. The subsequent positron annihilation, a secondary process, will create exiting photons (e.g., gammas) (Charlton and Humberston, 2001; Evans, 1982, p. 629). These photons can be considered as tertiary radiation. Pair-production is the dominant interaction at high energies as seen in Fig. 1.

The *photoelectric effect*, which is considered a primary process, happens when an incident photon is absorbed by an atom, causing the ejection or excitation of an orbital electron (Evans, 1982, p. 695). This responding orbital electron is considered a secondary electron. It is the dominant photon reaction at low energies (see Fig. 1).

Presently, MCATK does not have charged particle (especially electron) transport available. Due to this short-coming, MCATK does not account for the electron production of Bremsstrahlung photons. Also, MCATK is not modeling the fluorescence produced from the excitation casade of atomic electrons. To be clear, MCATK completely ignores the electrons (including any electron energy deposition) at this time.

Descriptions of each of the photoatomic processes and how they are implemented in MCATK will be explained in Subsections 2.1 to 2.4. Each subsection contains its subsubsections detailing the Monte Carlo implementation for each process.

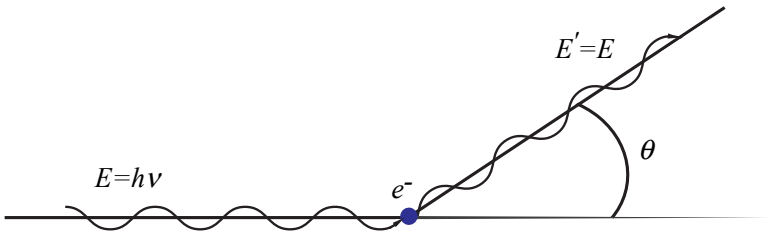

Figure 2: Illustration of coherent scattering. An incident photon of energy, $E = h\nu$, scatters off an electron and exits in a scattering cosine direction, $\cos\theta$, with an exiting energy equal to the incident energy, $E^{'} = E = h\nu$. (Based on Evans (1982))

2.1. Coherent Scattering

Elastic scattering of photons by bound atomic electrons is often called Rayleigh scattering (Roy et al., 1993, 1999; Evans, 1958, 1982) named after Lord Rayleigh who first described this type of light scattering (Strutt, 1871a,b). Other commonly used terms for Rayleigh scattering are explained by Roy et al. (1993),

> *Two other terms "elastic scattering" and "coherent scattering", have also been used interchangeably in discussing Rayleigh scattering. Although the two concepts are not identical, they can be used for Rayleigh scattering without much confusion as Rayleigh scattering is both elastic and coherent. By elastic scattering we mean that in the center of mass system of projectile and target the incident and final projectile energy are the same, which implies there is no transfer of energy between projectile and internal degrees of freedom of the target. On the other hand, by coherence we understand that it is only possible to define a cross section for a process that corresponds to a transition between observable initial and final states and that amplitudes for elastic scattering off different bound electrons must be added coherently.*

In this report, we will refer to Rayleigh scattering as *coherent scattering*.

Coherent scattering, physically, is when a photon incident on an electron will accelerate the electron, which in turn causes the electron to emit radiation. Fig. 2 illustrates this primary process that is often described as "scattering" of the incident photon. If the incident photon energy ($h\nu$) is much less than the target electron rest-mass energy ($m_e c^2$) then the emitted photon will have the same energy as the incident photon but does *not necessarily* emit along the incident direction. In the following subsubsections, we will build the coherent differential cross section and how it is sampled.

2.1.1. Thomson Cross Sections

Though Lord Rayleigh correctly predicted a $(1+\cos^2\theta)$ factor for the angular distribution of photon scattering (Strutt, 1871a,b), it would be Thomson (1903), using the classical theory of electromagnetic radiation and the theory of the electron who first accurately described a photon scattered off a free and at-rest electron. This process is described using the Thomson differential collision cross section and is defined by

$$\frac{d\left({}_e\sigma_{Thomson}\right)}{d\Omega} = T(\cos\theta) = \frac{{r_e}^2}{2}\left(1+\cos^2\theta\right), \tag{1}$$

where r_e is the *classical electron radius*[3] which is approximately equal to 2.8179 fm, the solid angle is $d\Omega = 2\pi \sin\theta \, d\theta$, and $\cos\theta$ is the exiting photon cosine direction as explained in Evans (1958, 1982).[4] $T(\cos\theta)$ is established here for later use in other sections. Eq. (1) is valid when the electron binding energy, B_e, is much smaller than the incident photon energy and the incident photon energy is in the classical limit ($B_e \ll h\nu \ll m_e c^2$).

For completeness, we include the Thomson total collision cross section (Thomson, 1903)[5] which is found by integrating the right-hand side of Eq. (1) over $d\Omega$ and which has the value

$$ {}_e\sigma_{Thomson} = \frac{8}{3}\pi {r_e}^2, \tag{2} $$

which is approximately equal to 0.6652 *barns*.

2.1.2. Coherent Cross Sections

In the previous subsubsection, "Thomson Cross Sections", the scattering description is for a photon interacting with a free and at-rest electron. A more general description needs to include the bound electron interactions which is the case for atoms. There are several good articles regarding the general case of coherent scattering of photons off atoms (Roy et al., 1999; Hubbell, 1999, 2006b). Using a common approximation, the Thomson differential collision cross section of Eq. (1) can be re-expressed with a scaling function as the coherent differential collision cross section and can be written as

$$ \frac{d({}_e\sigma_{coh})}{d\Omega} = C^2(Z, \mathrm{v}) \, T(\cos\theta). \tag{3} $$

Where $C(Z, \mathrm{v})$ is the coherent scattering function, often called the form factor, which is a function of atomic number, Z, and the momentum transfer $\mathrm{v} = K\alpha\sqrt{(1-\cos\theta)}$. Where $K = m_e c/\sqrt{2}\,h$ $[Angstroms^{-1}]$ and α $[unitless]$ is the incident energy, E, per electron rest-mass energy.

In general, the coherent form factors normalized by Z approaches the value of unity ($C(Z, \mathrm{v})/Z \to 1$) as $\mathrm{v} \to 0$, which means the binding energy is much less than the incident photon energy, $B_e \ll h\nu$, and the electron is basically a free at-rest electron and the coherent differential cross section becomes the Thomson differential cross section. The normalized form factor values fall off to zero ($C(Z, \mathrm{v})/Z \to 0$) as $\mathrm{v} \to \infty$ which means that $B_e \to \infty$, or the whole atom absorbs the incident photon momentum.

2.1.3. Sampling Coherent Scattering

In early released versions of the photon data libraries (`mcplibsXX`) the form factors were tabulated over the momentum transfer domain $0 < \mathrm{v} \leq 6$, and in more recent libraries (`eprdata12`) by Hughes (2013a,b,c), the data domain increases to $\mathrm{v} = 10^9$. To help visualize the coherent form factors and the two libraries tables differences, we plot in Fig. 3, the normalized form factors as

[3] Jackson (1975) explains the naming, "since a classical distribution of the charge totaling the electronic charge must have a radius of this order if its electrostatic self-energy is to equal the electron." Evans (1982) notes that, "This is not to be interpreted as having any significance in respect to the probable finite 'size' of an actual electron. Indeed, we have just seen that, in the derivation of the Thomson cross sections, the theory treated the electron as if it were a point charge."

[4] The units of Eq. (1) are $[cm^2/electron/steradian]$. $1\ barn = 100\ fm^2 = 10^{-24}\ cm^2$.

[5] Thomson's 1903 version had a factor of 2 error for the derivation of the total cross section [p. 268-271] which is corrected in the 1906 version.

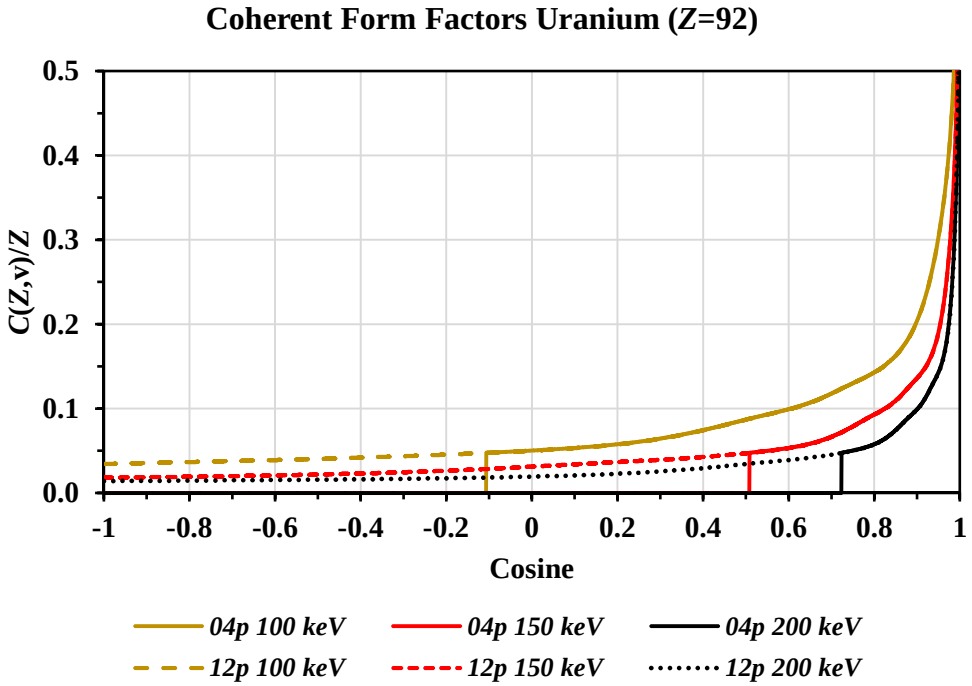

Figure 3: Coherent form factors ($C(Z,\mathrm{v})$) for Uranium, normalized by $Z = 92$, as a function of the scattering cosine. The labels *04p* and *12p* refer to the photon data libraries `mcplib04` and `eprdata12`, respectively. Shown are curves for incident photon energies of $E =$ 100, 150, and 200 *keV*. The `mcplibs04` form factors truncate to zero for cosines approximately at -0.1, 0.5, and 0.7 for incident photon energies of 100, 150, and 200 *keV*, respectively.

a function of cosine for $Z = 92$ and the three incident energies ($100, 150, 200$ *keV*). Note: The `mcplibs04` form factors truncate to zero for cosines approximately at -0.1, 0.5, and 0.7 for incident photon energies of 100, 150, and 200 *keV*, respectively. This is due to the shorter tabular domain of v for the `mcplibs04` coherent form factors compared to the `eprdata12` form factors.

Here we will describe the flow of the coherent scattering algorithm and point directly to MCATK software routines that handle this algorithm. For the C++ class, *CoherentScatterReaction*, the basic flow of sampling the coherent scattering in MCATK (which is found in the class function *SampleExitPhoton()*) is shown in Fig. 4. For coherent scattering it is more efficient to sample from the form factors, $C^2(Z,\mathrm{v})$, using an analytic interpolation[6] and using rejection on the normalized Thomson differential cross section term from Eq. (1). MCATK converts the momentum transfer, integrated form factor, and form factor data to the common logarithm (base-10) at setup time and uses those values in a corresponding analytic interpolation algorithm.

In Fig. 4, the input for the algorithm is the incident photon energy, E, and a random number generator, $\mathcal{R}$, while the output is the exiting scattered photon energy, $E' = E$, and scattering cosine ($\cos\theta$). The analytic interpolation is done in the class *CoherentScatterReaction* member functions, *calculateIntegratedFFSquaredMax()* and *sampleCosine()*.

[6]The analytic interpolation implemented by MCATK was communicated by G. Hughes, referred to in Hughes (2013a), and follows the implementation in MCNP6 (Goorley et al., 2012).

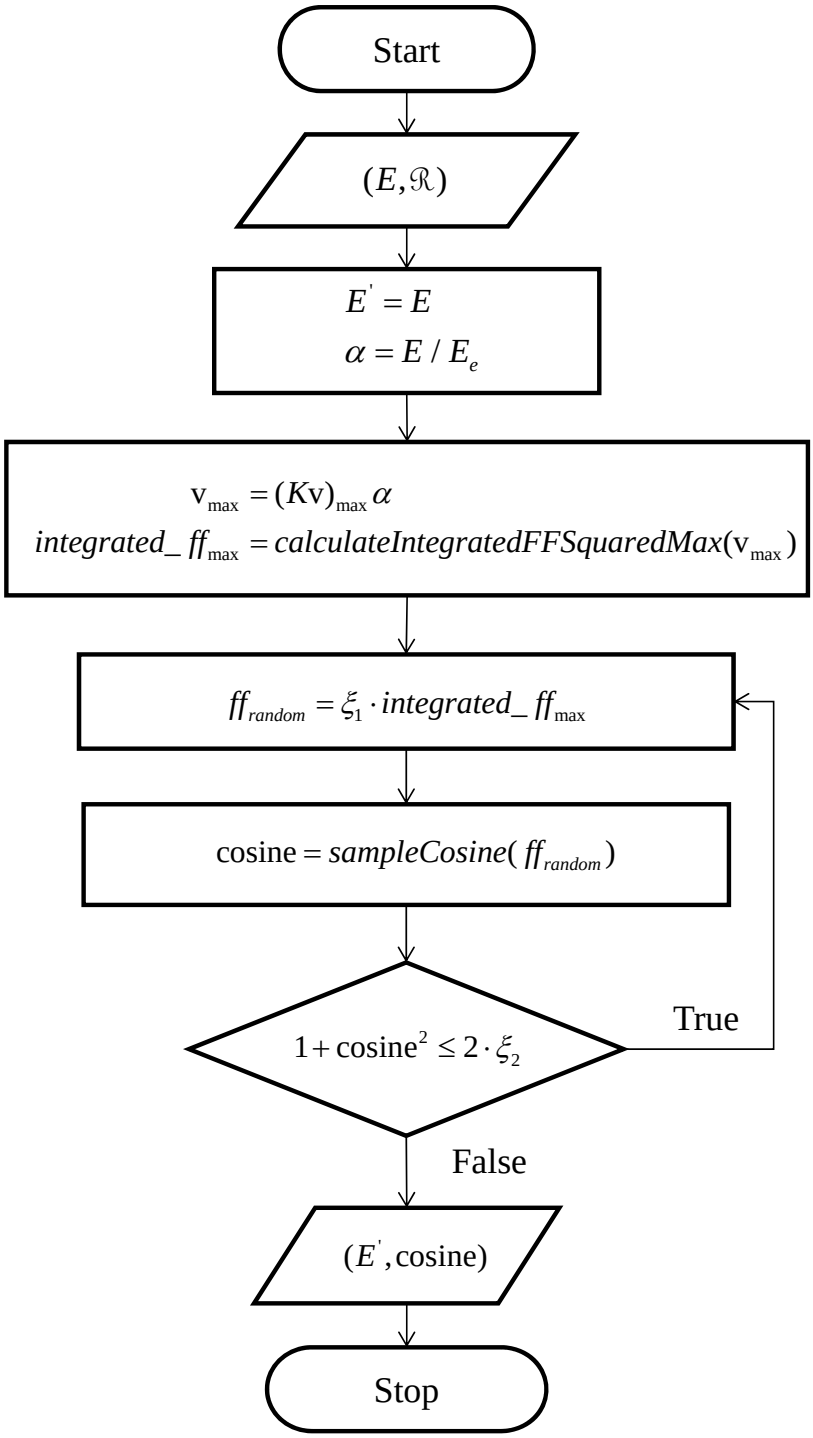

Figure 4: `CoherentScatterReaction::SampleExitPhoton()` : Flowchart for sampling the Coherent Scattering in MCATK. The inputs are the incident photon energy, E $[MeV]$ and the random number generator, $\Re$. The ξ_1 and ξ_2 are random numbers from the generator and E_e is the rest-mass energy of the electron. The outputs are the exiting photon energy, $E^{'} = E$ $[MeV]$, and scattering cosine. MCATK uses analytic interpolation in the `calculateIntegratedFFSquaredMax()` and `sampleCosine()` functions, and uses rejection on the normalized Thomson cross section term.Note: That $(K\mathrm{v})_{max} = \sqrt{2}\,K_{ff} = 41.2166$ and $K_{ff} = m_e c/(h\sqrt{2}) = 29.1445\ Angstroms^{-1}$.

2.1.4. Examples of Sampling Coherent Scattering

Within the MCATK testing framework is a "focused-integrated" test for the *CoherentScatterReaction::SampleExitPhoton()* function that can be called directly instead of with a fully integrated transport problem. The following Program 1 is an example of the test that was used to create the coherent exiting cosine distributions as seen in Figs. 5, 6, and 7. The sampling distributions are compared to the analytic coherent probability of scattering (PSC) in a given direction described by Eq. (A.1) in Appendix A.[7] All three figures were generated using the form factors from the data library `mcplib04`. The three MCATK sampled cosine distributions match nicely to the analytic coherent PSC.

Program 1 Sampling of the Coherent Scattering Cosine. Partial source code only.

```
TEST(SampleExitReaction_Coherent_Scattering) {

    CoherentScatterReaction CSC(Data_mcplib04);
    Tally tally;

    for(auto i=0; i<Samples; ++i) {
       Rxn::Result Exit_results =
         CSC.SampleExitPhoton( incomingEnergyMeV, rand );

       tally.Binning( Exit_results.cosine );
    }
    std::vector<double> Bins = tally.getDistribution();
}
```

For Fig. 5, the two coherent methods at an incident energy of 0.0011 MeV match each other well. At this energy, the limited momentum transfer, v, domain of the coherent form factors for Uranium, is not a factor in the distributions.

In Figs. 6 and 7, the two methods follow each other fairly well. However, unlike the previous figure, the limited momentum transfer domain in the coherent form factors is demonstrated as the distributions drop to zero at approximately Cosine $= 0.5$ and 0.99, respectively. The black circle distribution is matching the coherent PSC curve (in red) at that transition.

[7] For comparing to the sampled distributions, the PSC calculated was the unnormalized probability, $p_{coh}(Z,E,\mu)\ \sigma_{coh}(Z,E)$.

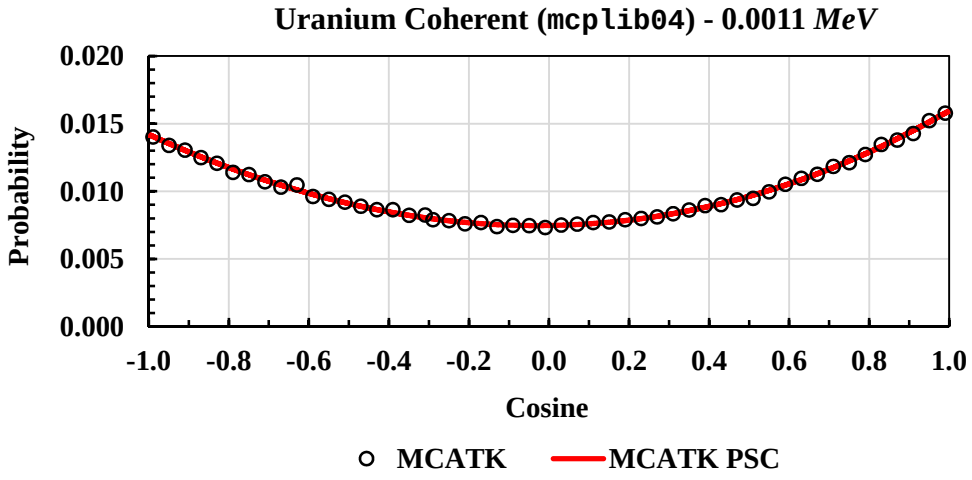

Figure 5: Uranium coherent scattering cosine distribution at $E = 0.0011\ MeV$. The MCATK sampling from the *CoherentScatterReaction::SampleExitPhoton()* function compared to the analytic probability of scattering (PSC).

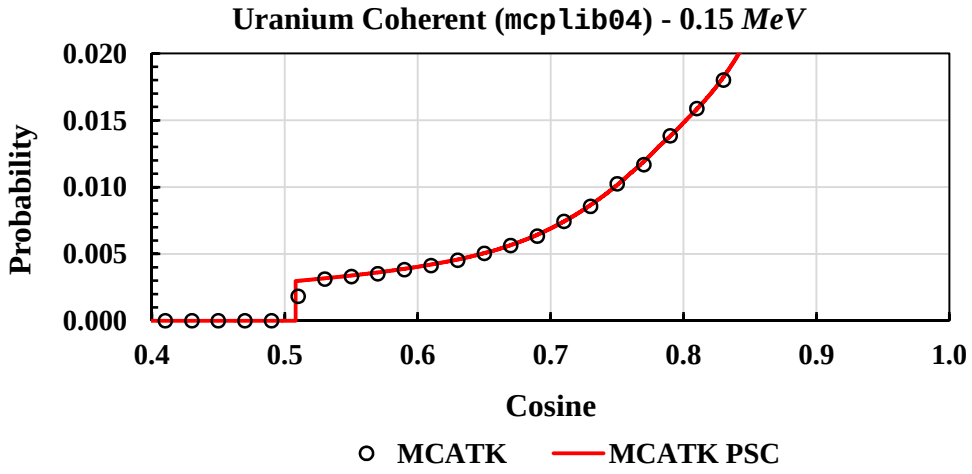

Figure 6: Uranium coherent scattering cosine distribution at $E = 0.15\ MeV$. The MCATK sampling from the *CoherentScatterReaction::SampleExitPhoton()* function compared to the direct analytic probability of scattering (PSC). Note: The cosine domain view has been reduced from -1.0 to 1.0 to just 0.40 to 1.00.

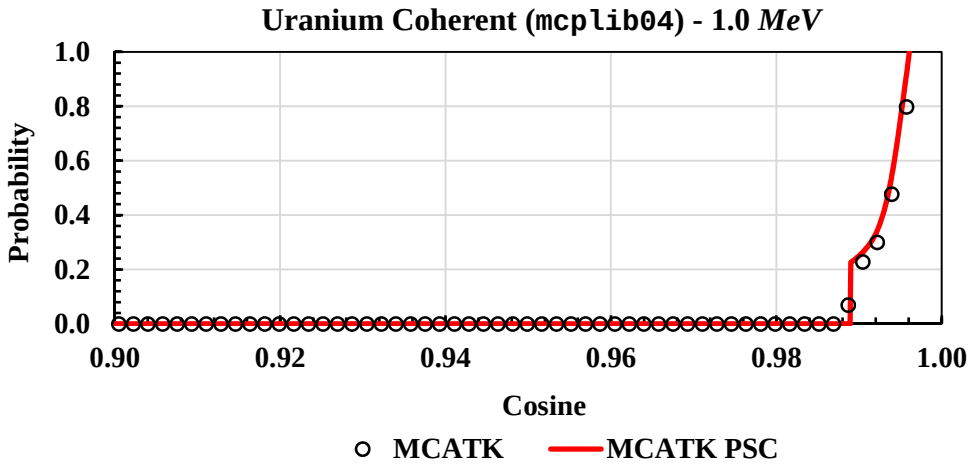

Figure 7: Uranium coherent scattering cosine distribution at $E = 1.0\,MeV$. The MCATK sampling from the `CoherentScatterReaction::SampleExitPhoton()` function compared to the direct analytic probability of scattering (PSC). Note: The cosine domain view has been reduced from -1.0 to 1.0 to just 0.90 to 1.00.

2.2. *Incoherent Scattering*

Incoherent scattering, in the case of a photon off of an atom (more specifically a charged particle, usually an electron), means the outgoing photon will *no longer* have the same phase and frequency of the incident photon. This is commonly known as Compton scattering (Compton, 1923), where in some cases the exiting photon has a decreased energy compared to the incident energy of the photon as seen in Fig. 8. The exiting photon is accompanied by an exiting recoil electron that has absorbed the energy difference between the incident photon and exiting photon which conserves the total energy in the system. The total energy conservation equation can be written as

$$E + E_e = E^{'} + E_e^{'}, \tag{4}$$

where E is the incident photon energy, E_e is the rest-mass energy of the electron, $E^{'}$ is the exiting photon energy, and $E_e^{'}$ is the exiting recoil electron energy which is the sum of kinetic energy plus rest-mass energy. Note: Since the target electron take on kinetic energy that is equal to the difference between the incident photon and exiting photon, then the collision is considered an *inelastic* scattering event. Photon scattering at very low photon energies ($h\nu \ll E_e$) off a free and at-rest electron is described by the non-relativistic classical theory of Thomson (as previously presented in Subsection 2.1). But as the photon energy, $h\nu$, approaches the rest-mass energy of the electron, $m_e c^2$, the relativistic corrections quickly become important. The exiting photon energy ($E^{'} = h\nu^{'}$) is given by the Compton-Debye energy shift formula (Compton, 1923; Debye, 1923, 1954)

$$E^{'} = E[1 + \alpha(1 - \cos\theta)]^{-1}, \tag{5}$$

where $E = h\nu$ is the incident photon energy, $\alpha = E/E_e$ is the normalized incident photon energy, and $\cos\theta$ is the scattering cosine of the photon.[8]

[8]Though the Compton-Debye wavelength shift is independent of the incident photon energy, it is important to note that the energy shift is strongly dependent on the incident photon energy.

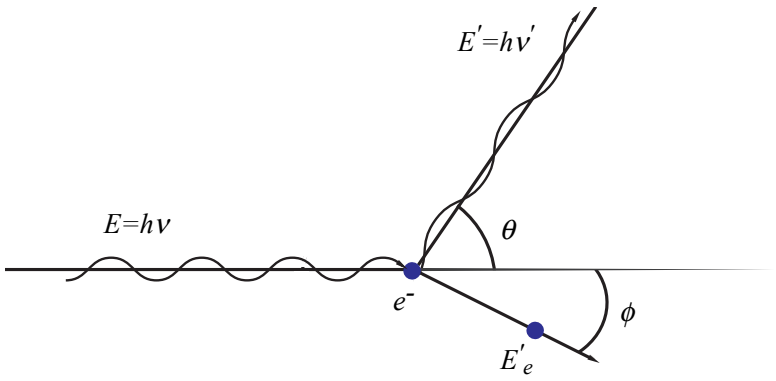

Figure 8: Illustration of Basic Incoherent Scattering. An incident photon of energy, $E = h\nu$, scatters off an electron. Exiting is a photon with scattering cosine, $\cos\theta$, and an exiting energy, $E^{'} = h\nu^{'}$. Accompanying the exiting photon is a recoiling electron with an scattering cosine, $\cos\phi$, and an energy, $E_e^{'}$. (Based on Evans (1982))

2.2.1. Klein-Nishina Cross Section

In 1929, Klein and Nishina (1929, 1994) provided a differential scattering cross section for Compton scattering. Their derivation, often called the Klein-Nishina formula, was one of the first successful applications from the study of quantum electrodynamics (QED) and is one of the earliest confirmations of the Dirac electron theory (Evans, 1982; Brown, 2002). The Klein-Nishina formula is an approximation that is exact for a free and at-rest electron.

The Klein-Nishina differential collision cross section formula for *unpolarized* photons[9]

$$\frac{d({}_e\sigma_{KN})}{d\Omega} = \frac{{r_e}^2}{2}\left(1+cos^2\theta\right)\left[\frac{1}{1+\alpha(1-\cos\theta)}\right]^2\left\{1+\frac{\alpha^2(1-\cos\theta)^2}{(1+cos^2\theta)\left[1+\alpha(1-cos\theta)\right]}\right\}, \quad (6)$$

where r_e is the classical electron radius.[10] Note: That at low energies ($\alpha \ll 1$), Eq. (6) reduces to the classical non-relativistic Thomson differential collision cross section formula described in Eq. (1).

Sometimes it is more convenient to write the Klein-Nishina differential collision cross section in an energy (or frequency) form (Evans, 1982, p.683). By using Eq. (5) then Eq. (6) can be re-written as

$$\frac{d({}_e\sigma_{KN})}{d\Omega} = K(E,\cos\theta) = \frac{{r_e}^2}{2}\left(\frac{\alpha^{'}}{\alpha}\right)^2\left(\frac{\alpha}{\alpha^{'}}+\frac{\alpha^{'}}{\alpha}+1-\cos\theta\right), \quad (7)$$

where α and $\alpha^{'}$ are the incoming and exiting photon energy per electron rest-mass energy ($m_e c^2$), respectively.[11] $K(E,\cos\theta)$ is established here for later use in other sections.

[9] A more general form of the Klein-Nishina formula is for a source of incident polarized photons and is described by Evans (1982). For more on polarization effects and photon transport then see Fernández et al. (1993) and Ramella-Roman et al. (2005).

[10] See Evans (1958, 1982) for more details about the physical meaning of certain terms in Eq. (6).

[11] The units for Eqs. (6) & (7) are in $[cm^2/electron/steradian]$.

For completeness, the total collision cross section is presented.[12] The Klein-Nishina total collision cross section is found by integrating the right-hand side of Eq. (6) or Eq. (7) over $d\Omega$ and gives the form

$$ {}_e\sigma_{KN} = 2\pi {r_e}^2 \left\{ \frac{1+\alpha}{\alpha^2} \left[\frac{2(1+\alpha)}{1+2\alpha} - \frac{1}{\alpha} ln(1+2\alpha) \right] + \frac{1}{2\alpha} ln(1+2\alpha) - \frac{1+3\alpha}{(1+2\alpha)^2} \right\}. \tag{8} $$

This cross section[13] is described by Evans (1958, p. 684), "The total (or average) collision cross section is the probability of removal of the photon from a collimated beam while passing through an absorber containing one $electron/cm^2$." For small values of α, a power series gives

$$ {}_e\sigma_{KN} = \frac{8\pi}{3} {r_e}^2 \left(1 - 2\alpha + \frac{26}{5}\alpha^2 - \frac{133}{10}\alpha^3 + \ldots \right). \tag{9} $$

This series can be useful when Eq. (8) becomes numerically unstable at smaller values of α.[14] It is easy to see from this series expansion that as α goes to zero, the Klein-Nishina total collision cross section goes to the Thomson total collision cross section in Eq. (2). The expansion coefficients for Eq. (9) can be found using the formula

$$ D_n = \frac{(-2)^n (16 + 22n + 17n^2 + 8n^3 + n^4)}{6 + 11n + 6n^2 + n^3}, \tag{10} $$

where $n \geq 0$ and is integer values. Eq. (10) was found with Wolfram Research, Inc. (2015) using Mathematica's `SeriesCoefficient()` function applied to Eq. (8). For the total Klein-Nishina cross section formula, when the incident $\alpha < 0.125$, the power series expansion in Eq. (9) is used. In MCATK, Horner's rule is used to evaluate this polynomial (Horner, 1819; Knuth, 1998, p. 486).

2.2.2. *Incoherent Cross Section*

As shown in the subsubsection on Thomas scattering cross section, the Klein-Nishina cross section assumes the scattering description is for a photon interacting with a free and at-rest electron. A more general description needs to include the bound electron interactions for the case of atoms (Veigele et al., 1966; Hubbell, 1997, 2006b). The Klein-Nishina differential collision cross section of Eq. (7) can be re-expressed by applying a scaling function to the Klein-Nishina differential equation into what is called an incoherent differential collision cross section as

$$ \frac{d({}_e\sigma_{incoh})}{d\Omega} = I(Z, \mathrm{v})\, K(E, \cos\theta), \tag{11} $$

where $I(Z, \mathrm{v})$ is the incoherent form factors, which is a function of atomic number, Z, and the momentum transfer, v, as defined after Eq. (3).

In general, the incoherent form factors normalized by Z drops to the value of zero ($I(Z, \mathrm{v})/Z \to 0$) as $\mathrm{v} \to 0$, or the whole atom absorbs the momentum. The normalized form factor values approaches unity ($I(Z, \mathrm{v})/Z \to 1$) as $\mathrm{v} \to \infty$ which means that B_e is negligible compared to the incident photon energy, $B_e \ll h\nu$, which means the electron is basically a free at-rest electron and the incoherent differential cross section becomes the Klein-Nishina differential cross section.

[12] Though the MCATK library has available the use of the Klein-Nishina total collision cross section, it is not being directly used at this time in our photon algorithms.

[13] Eq. (8) is the same for *both polarized and unpolarized* incident radiation and has units of $[cm^2/electron]$.

[14] Eq. (8) is numerically unstable due to the near cancellation of the *logarithm* and *algebraic* terms.

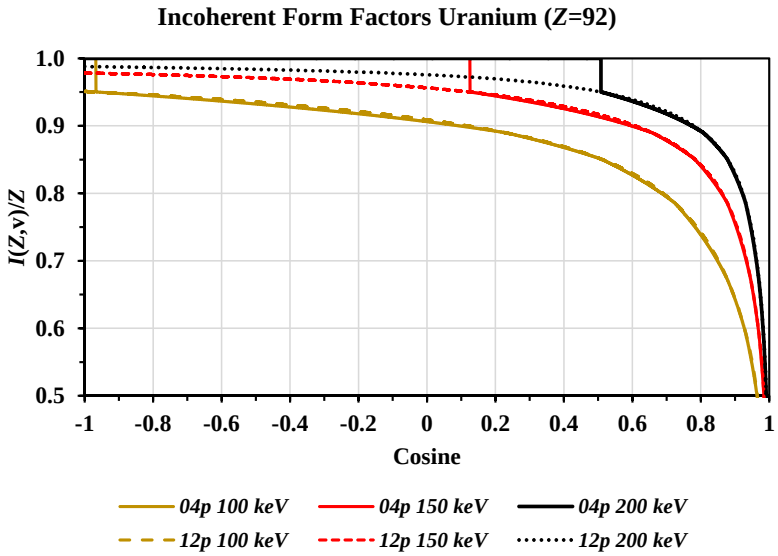

Figure 9: Incoherent form factors ($I(Z,\nu)$) for Uranium, normalized by $Z = 92$, as a function of the scattering cosine. The labels *04p* and *12p* refer to the photon data libraries `mcplib04` and `eprdata12`, respectively. Shown are curves for incident photon energies of $E =$ 100, 150, and 200 *keV* for each library.

2.2.3. Sampling Incoherent Scattering

As mentioned previously in Subsubsection 2.1.3: "Sampling Coherent Scattering", the earlier versions of the photon data libraries (`mcplibsXX`) have limited momentum transfer domain. Similarly the incoherent form factors are tabulated over a limited momentum transfer domain, in this case, $0 < \nu \leq 10$. But in more recent libraries (`eprdata12`) by Hughes (2013a,b,c) the momentum transfer domain is up to $\nu = 10^9$. To help visualize the incoherent form factors and how the two library tables differ, we plot in Fig. 9 the normalized form factors as function of cosine for $Z = 92$ and three incident energies $(100, 150, 200\ keV)$. Note: The `mcplibs04` form factors are forced to unity for decreasing cosines approximately at -0.98, 0.11, and 0.5 and for incident photon energies of 100, 150, and 200 *keV*, respectively. This is due to the shorter tabular domain of ν for the `mcplibsXX` incoherent form factors compared to the `eprdata12` form factors.

The logic flow for calculating the resulting photon energy and direction from incoherent scattering in MCATK is given in Fig. 10. The MCATK C++ class is *`IncoherentScatterReaction`*. Unlike the coherent sampling, in the class function *`SampleExitPhoton()`*, we sample for an exiting energy and direction from the Klein-Nishina cross section in the class function *`SampleKleinNishina()`* and base rejection on the incoherent form factor. To perform the sampling of the Klein-Nishina differential cross section, the two sampling methods by Kahn (1956) and Koblinger (1975) are implemented and called from the member function *`SampleKleinNishina_General()`* [15] which uses the Kahn method for $\alpha < 3.0$ and Koblinger Method for $\alpha \geq 3.0$. The combined use of these two methods is suggested by Blomquist and Gelbard (1983). The incoherent momen-

[15] MCATK uses an analytical model for Hydrogen in member function *`SampleKleinNishina_Hydrogen()`*

tum transfer and form factor data have been converted to common logarithm (base-10)[16], so the use of linear-linear interpolation for the incoherent form factors is performed in the function *IncoherentScatterReaction::IncoherentFF()*.

The MCATK implementation of the Kahn (1956) sampling method is illustrated by the flowchart in Fig. 11. The method has an input of α and a random number generator, $\mathcal{R}$, and an output of a suggested exiting α' and a scattering cosine. At this time, we do not allow an incoming α under a value of $1x10^{-7}$ due to extreme inefficiencies in sampling. It has been shown by Blomquist and Gelbard (1983) that the Kahn method is fairly efficient (~ 60 *percent*) at $\alpha < 3$. For $\alpha \geq 3$, more efficient alternative methods were suggested to replace the Kahn method and we chose the Koblinger (1975) method, as described in Fig. 12.

[16]MCATK uses v = *std::numeric_limits<double>::min()* when v = 0 since the logrithm of zero is not defined.

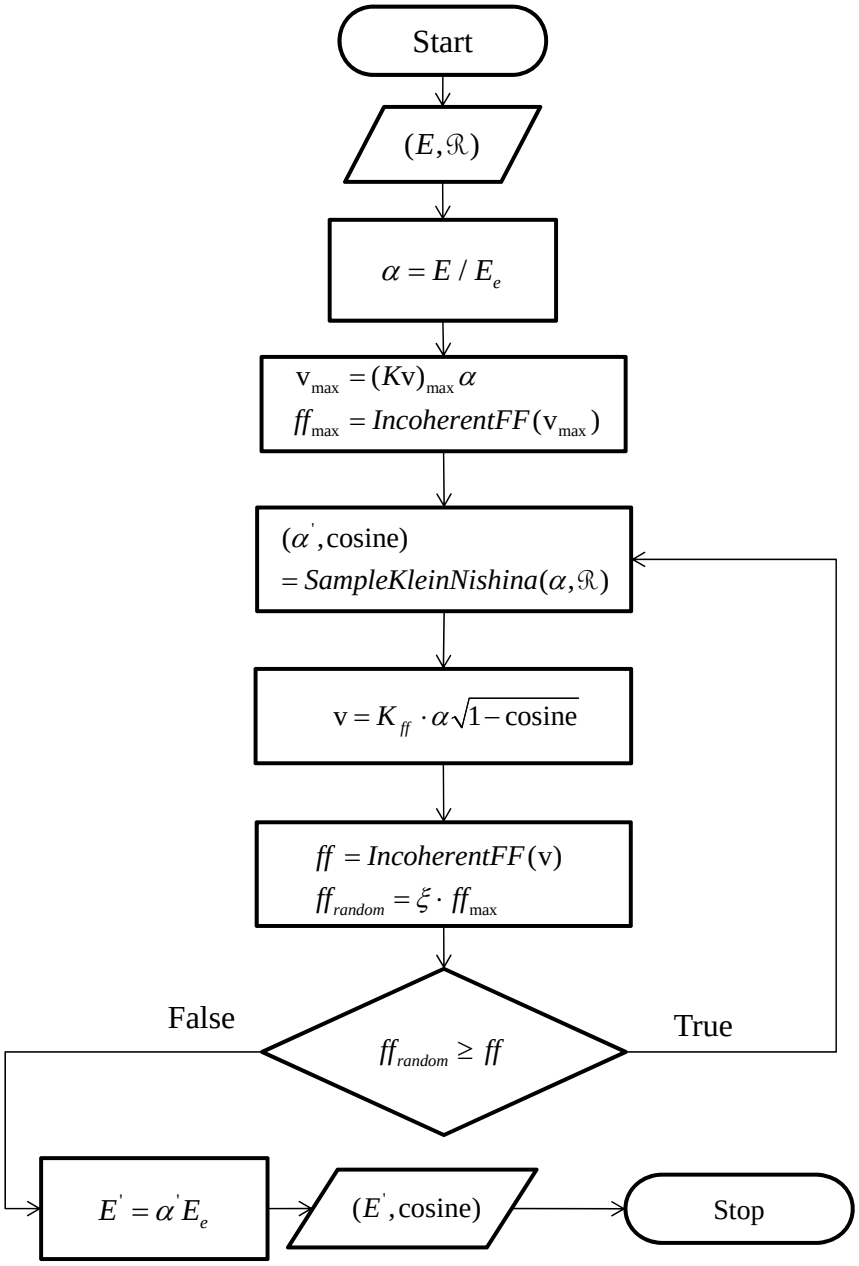

Figure 10: `IncoherentScatterReaction::SampleExitPhoton()`: Flowchart for sampling the incoherent scattering in MCATK. The inputs are the incident photon energy, E $[MeV]$, and the random number generator, $\Re$. The ξ is the random number from the generator. E_e is the rest-mass energy of the electron. The outputs are the exiting photon energy, $E^{'}$ $[MeV]$ and the scattering cosine. Note: We sample the Klein-Nishina cross section and perform rejection of the incoherent form factor, ff. Note: That $(K\mathrm{v})_{max} = \sqrt{2}\,K_{ff} = 41.2166$ and $K_{ff} = m_e c/(h\sqrt{2}) = 29.1445\ Angstroms^{-1}$.

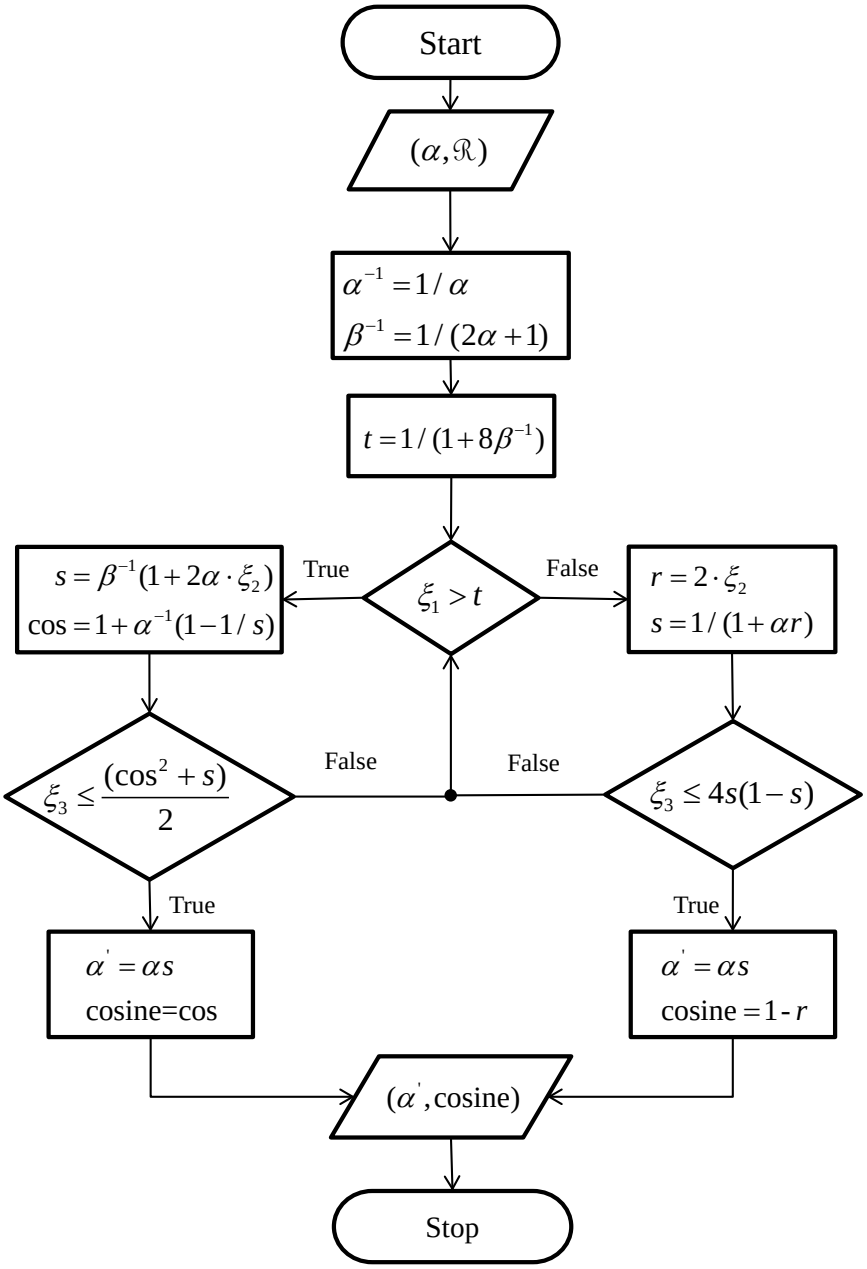

Figure 11: *KahnMethod()* : Flow of Kahn sampling method (Kahn, 1956) for selecting an energy and scattering cosine for Klein-Nishina sampling in MCATK for $\alpha < 3$. The inputs are the scaled and unitless incident photon energy, α, and the random number generator, $\Re$. The ξ_i are the random numbers from the generator. The outputs are the exiting photon energy, α' and the scattering cosine.

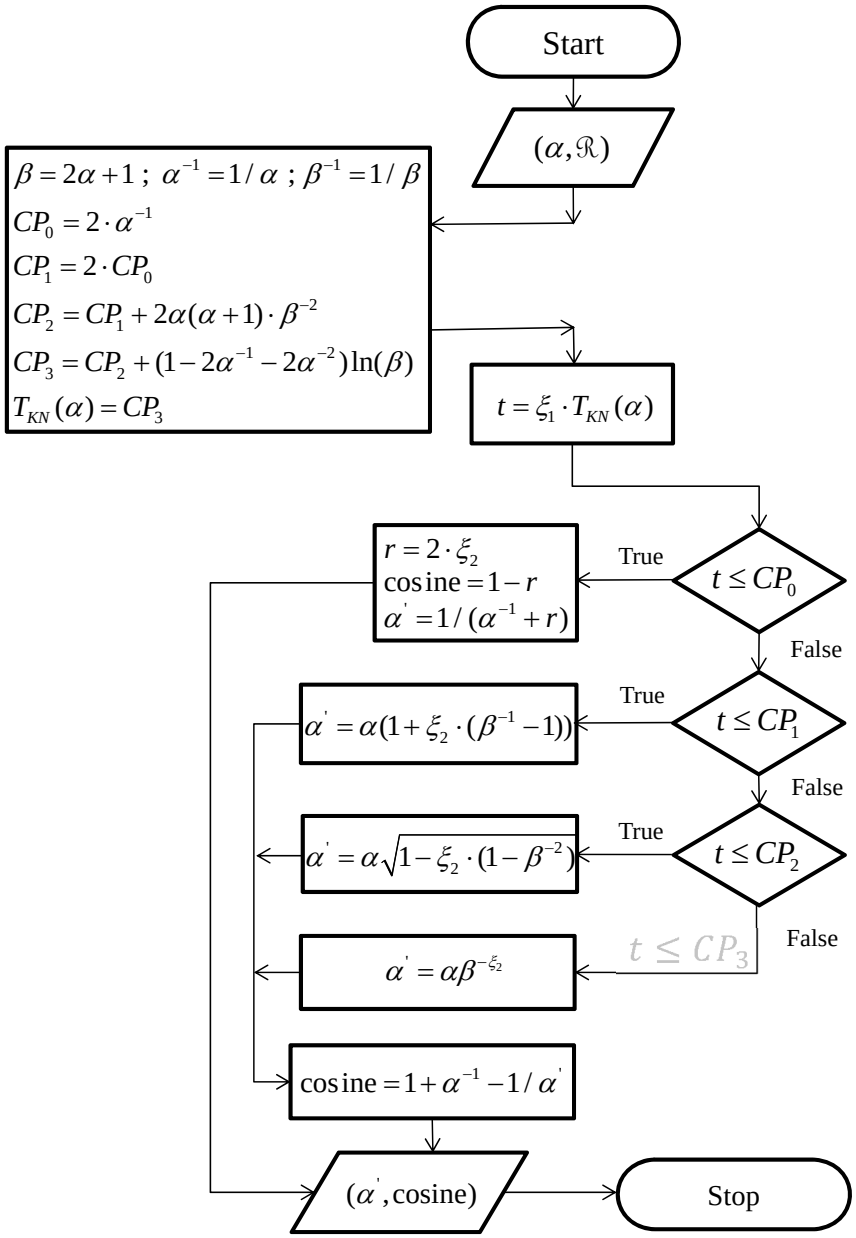

Figure 12: *KoblingerMethod()* : Flow of Koblinger (direct) sampling method (Koblinger, 1975) for selecting an energy and scattering cosine for Klein-Nishina sampling in MCATK for $\alpha \geq 3$. The inputs are the scaled and unitless incident photon energy, α, and the random number generator, $\Re$. The ξ_i are the random numbers from the generator. The outputs are the exiting photon energy (α') and the scattering cosine.

2.2.4. Examples of Sampling Incoherent Scattering

Following closely the sampling of coherent scattering in Subsubection 2.1.4, we tested the sampling of the incoherent scattering. So, within the MCATK testing framework we setup a "focused-integrated" test that could be called explicitly, and not in a fully integrated transport problem, for the *IncoherentScatterReaction::SampleExitPhoton()* function. The following Program 2 is an example of the test that was used to sample for the incoherent exiting cosine distributions and energy as seen in Figs. 13, 14, and 15 and the Figs. 16, 17, and 18, respectively. All six figures were generated using the form factors from the data library `mcplib04`.

The Figs. 13, 14, and 15 show the scattering cosine distribution for incident energies of 0.0011, 0.15, and 1.0 *MeV*, respectively. The sampling of the scattering cosine distributions are compared to the incoherent analytic probability of scattering (PSC) in a given direction as described by Eq. (A.5) in Appendix A.[17]

Program 2 Sampling of the Incoherent Scattering Cosine. Partial source code only.

```
TEST(SampleExitReaction_Incoherent_Scattering) {

    IncoherentScatterReaction ISC(Data_mcplib04);
    Tally tally;

    for(auto i=0; i<Samples; ++i) {
       Rxn::Result Exit_results =
          ISC.SampleExitPhoton( incomingEnergyMeV, rand );
          tally.Binning(Exit_results.cosine);
    }
    std::vector<double> Bins = tally.getDistribution();
}
```

All of the MCATK (sampled) and MCATK PSC curves match well. Note: For an energy of 0.15 *MeV* in Fig. 14 at about a cosine of 0.1, there is a "small kink" in the MCATK and MCATK PSC distributions. This is from the limited domain of the momentum transfer, v = 10, for the incoherent form factors. It is not very pronounced due to the scaling of the plot and the figure.

The MCATK sampling of the energy distributions is compared to MCNP6 results. The Figs. 16, 17, and 18 show the exiting photon energy distributions for incident energies of 0.0011, 0.15, and 1.0 *MeV*, respectively. In Fig. 16, for an energy of 0.0011 *MeV*, both MCATK and MCNP6 could use a finer binning structure. For MCNP6, we used the PTRAC files which proved to be somewhat more difficult to obtain the needed samplings at these smaller energy ranges. At the other two energies the MCATK and MCNP6 curves match well.

[17] For comparing to the sampled distributions, the PSC calculated was the unnormalized probability $p_{incoh}(Z, E \rightarrow E', \mu)\ \sigma_{incoh}(Z, E)$.

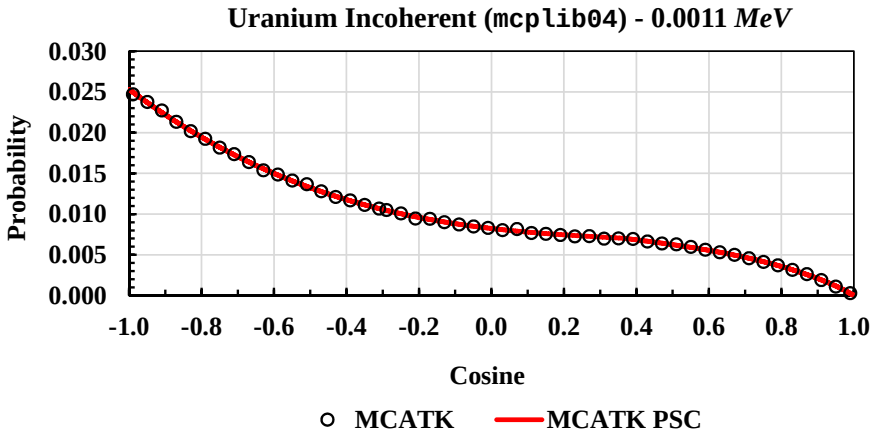

Figure 13: Uranium incoherent scattering cosine distribution at $E = 0.0011\ MeV$.

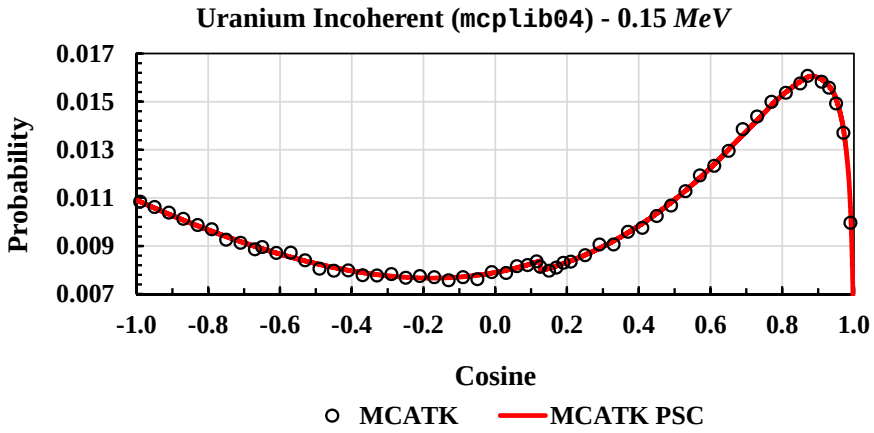

Figure 14: Uranium incoherent scattering cosine distribution at $E = 0.15\ MeV$.

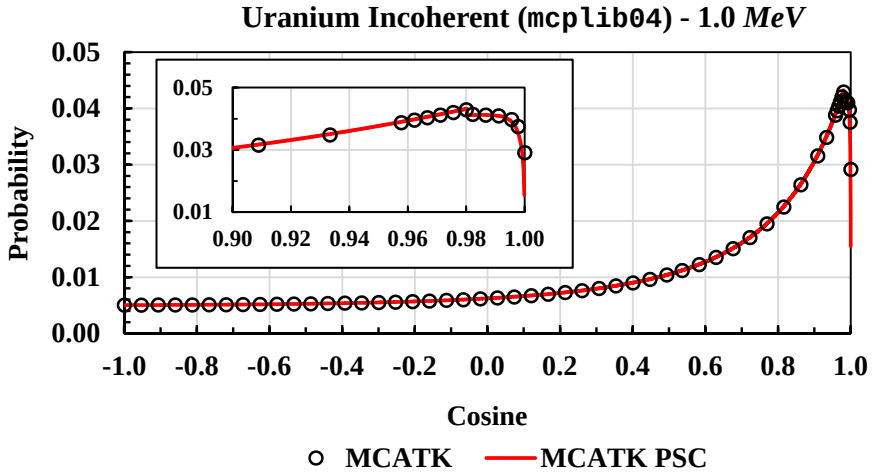

Figure 15: Uranium incoherent scattering cosine distribution at $E = 1.0\ MeV$.

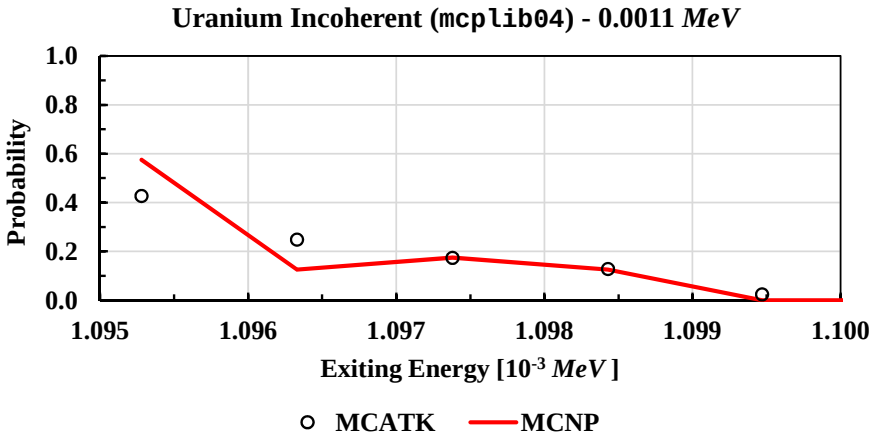

Figure 16: Uranium incoherent exiting energy distribution for an incident photon at $E = 0.0011\ MeV$.

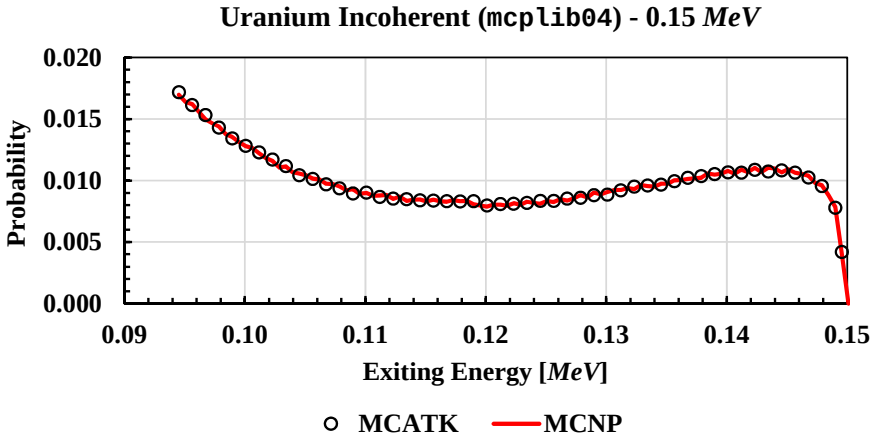

Figure 17: Uranium incoherent exiting energy distribution for an incident photon at $E = 0.15\ MeV$.

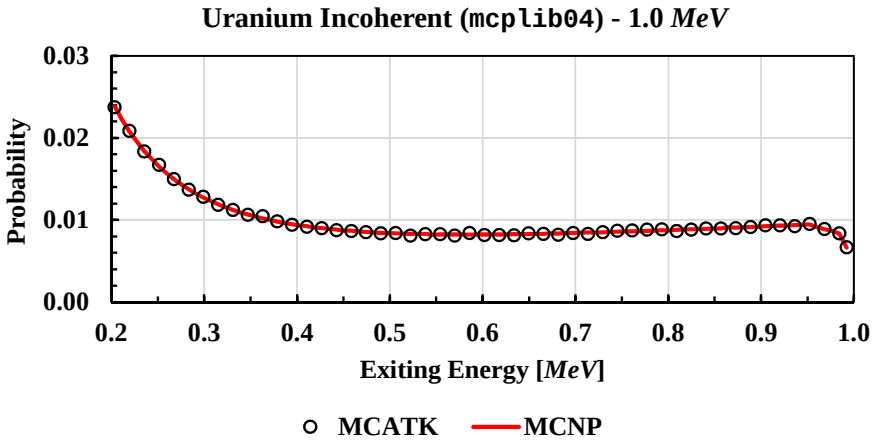

Figure 18: Uranium incoherent exiting energy distribution for an incident photon at $E = 1.0\ MeV$.

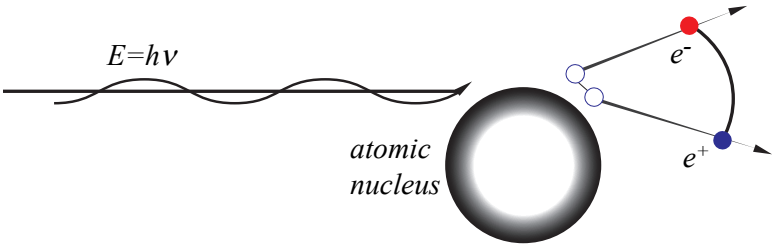

Figure 19: Illustration of pair-production. An incident photon with energy of at least, $E = h\nu = 2E_e$ interacts with the field of an atomic nucleus to spontaneously produce an electron-positron pair. (Based on Evans (1982))

2.3. Pair-Production

Pair-production is a primary process which occurs when a photon with energy at least twice that of the rest-mass energy of an electron (i.e., an energy greater than $\sim 1.022\ MeV$) interacts with the field of an atomic nucleus, as in Fig. 19, to spontaneously produce an electron-positron pair (Evans, 1982; Charlton and Humberston, 2001; Hubbell, 2006a). The incident photon energy is completely absorbed and the particle pair is produced through energy creation. Pair-production is the dominant photon interaction of the four possible interactions at high energies, see Fig. 1. The created electron-positron pair has a total kinetic energy equal to the incident photon energy minus twice the electron rest-mass energy. The particles decelerate through the system (generating Bremsstrahlung photons as they do so) until the positron annihilates with an electron. The annihilation *generally* leads to the emission of two 0.511 MeV photons (which is considered tertiary radiation) traveling in opposite directions (Charlton and Humberston, 2001; Evans, 1982, p. 629).

2.3.1. Annihilation Photon Production

Positron annihilation is a secondary process. Since MCATK is *not* capable of charged particle transport at this time, it is *assumed* the annihilation occurs at the incident photon collision site. The direction for the first photon is sampled isotropically, and the second photon is emitted in the opposite direction from the first. Each photon is emitted with 0.511 MeV.[18] It is important to note that without a charge particle transport capability, Bremsstrahlung photons are not created and transported in MCATK and the photon flux may be underestimated depending on the problem of interest.

There are several annihilation state configurations possible, but nearly all annihilation radiation comes from the singlet-state and produces two photons. The other configurations have extremely low probabilities (Charlton and Humberston, 2001; Hubbell, 2006a; Evans, 1982, p. 629)

2.4. Photoelectric Effect (Absorption)

The photoelectric effect, which is considered a primary process and is illustrated in Fig. 20, occurs when an incident photon is absorbed by an atom, causing the ejection or excitation of an orbital electron (Einstein, 1905, 1967; Millikan, 1916). It is the dominant photon reaction at low energies, see Fig. 1. The de-excitation of an excited electron can lead to the emission of

[18] MCATK implementation uses a electron rest-mass energy of 0.510998910 MeV.

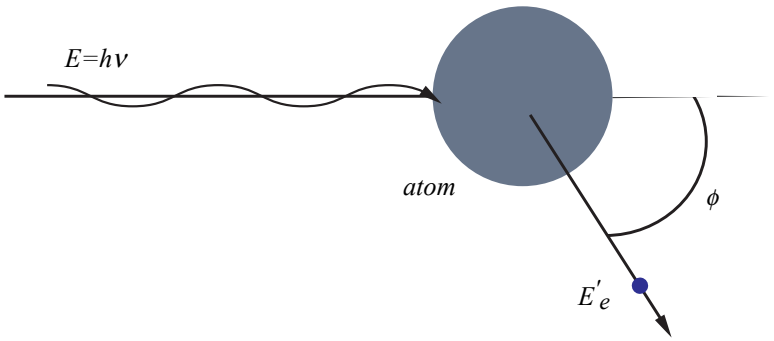

Figure 20: Illustration of photoelectric effect. An incident photon, $E = h\nu$, is absorbed by an atom, causing the ejection, $E_e^{'}$ or excitation of an orbital electron. (Based on Evans (1982))

some number of fluorescent photons, while the deceleration of an ejected electron will generate Bremsstrahlung photons (Carter and Cashwell, 1977; Evans, 1982; Lux and Koblinger, 1991; Turner, 1992).

However, since neither fluorescence, nor charged particle transport, nor a thick-target Bremsstrahlung model (Emigh, 1970; Evans, 1982, p.614) is implemented in MCATK at this time, photoelectric events in MCATK are modeled as *simple absorption* of the incident photon.

3. Photon Production From Neutron Interactions

Many neutron interactions result in the emission of one or more photons $(n,x\gamma)$, e.g., inelastic scatter, fission, capture, etc. The data describing photon emissions are contained in the neutron continuous energy ACE (A Compressed ENDF) files (MacFarlane and Muir, 1997) rather than with the continuous energy photon data.

Detailed photon production data does not exist for every possible interaction type that a neutron may undergo with every isotope. Thus, the photon production data is often lumped into one or several aggregate data tables. As a result, photon production events cannot be correlated to the actual neutron interaction event that occurred in the simulation; the data may simply not exist. Instead, the expected number of photons generated across all possible interactions for the incident neutron energy is obtained. Photons may be generated even if the sampled neutron collision is of a type that does not, in reality, produce any photons. For each photon generated, which may be more than one per reaction, an exit state is sampled from the available photon production table or tables. The exit state may correspond to a completely different reaction than that actually undergone by the neutron, and it often corresponds to a different reaction than those sampled for other photons created by the same neutron event. This method of generating photons leads to the correct expected behavior, provided that enough neutron histories are simulated.

In order to limit the amount of time spent tracking photons, particularly in fissile regions in which many photons are created per collision, the number of Monte Carlo photons generated by neutron interactions is reduced. The weights of the new photons are increased to preserve the correct physical number of photons created. MCATK uses a simplified version of an algorithm taken from MCNP5 (X-5 Monte Carlo Team, 2003 Revised 2/1/2008) to reduce the number of Monte Carlo photons created in each collision. If the expected number of photons is less than 1, then the number

of Monte Carlo photons created, N_{MC}, is

$$N_{MC} = \lfloor N + \xi \rfloor, \tag{12}$$

where N is the expected number of photons and ξ is a pseudo-random number between 0 and 1. If the expected number of photons is greater than 1, then the number of Monte Carlo photons created is

$$N_{MC} = MIN(10, \lfloor N/5 + 1 \rfloor). \tag{13}$$

So, if the expected number of photons is greater than 1, then roughly one-fifth as many Monte Carlo photons will be generated, and the number generated will always be between 1 and 10.

4. Verification Examples

We present some basic examples of verification work that was done as the photon physics was implemented. These examples are not exhaustive and are only a small sampling of the unit and integrated testing done to the photon transport implemention. In the following subsections (4.1 and 4.2), we will briefly discuss our collision and flux tally results, respectively.

4.1. Collision Tallies

After adding the sampling of gamma particles from neutron induced reactions (ie., $(n,x\gamma)$), we demonstrate the accuracy of the sampling and tracking implementation with a K_{eff} eigenvalue problem using coupled neutron-gamma physics and compare the behavior to MCNP6 values out of the "Problem Summary Tables" in the following tables. The problem geometry consists of a sphere of Uranium surrounded by a spherical shell of water. The neutron and gamma event tallies are presented in Tables 1 and 2, respectively. The results show excellent agreement ($\sim< 2\%$) between the traditionally available neutron events, and also for the recently available photon events. The relative percent difference in Compton events from Table 2 shows 2.58 percent less scores for MCATK, but this is directly related to current design decisions in MCATK to treat photoelectric events as terminal without generating any secondary photons. Because MCNP6 generates and tracks these secondary photons and because a small fraction of these will undergo Compton collisions, its Compton collision count will naturally be higher. However, due to the low energy of such photons, the actual amount of total energy loss in the Compton events is virtually identical between the two codes.

Table 1: Comparison of MCATK and MCNP6 *neutron* collision tallies from a K_{eff} calculation of a Uranium sphere surrounded by water. Energy is in units of $[MeV]$. $|(MCNP - MCATK)|/MCNP$

Neutrons	MCATK			MCNP6			Relative % Difference		
Event	**Count**	**Weight**	**Energy**	**Count**	**Weight**	**Energy**	**Count**	**Weight**	**Energy**
source	2503131	1.00000	2.04458	2500127	1.00000	2.03590	0.12	0.00	0.43
(n,xn)	9277	0.00371	0.00255	9128	0.00365	0.00249	1.63	1.52	2.11
fission	1000490	0.39969	0.42373	998639	0.39943	0.42125	0.19	0.07	0.59
capture	1421573	0.56792	0.02877	1421768	0.56868	0.02881	0.01	0.13	0.13
leakage	85709	0.03424	0.03365	84287	0.03371	0.03297	1.69	1.57	2.06

Table 2: Comparison of MCATK and MCNP6 *photon* collision tallies from a K_{eff} calculation of a Uranium sphere surrounded by water. Energy is in units of $[MeV]$. $|(MCNP - MCATK)|/MCNP$

Photons	MCATK			MCNP6			Relative % Difference		
Event	**Count**	**Weight**	**Energy**	**Count**	**Weight**	**Energy**	**Count**	**Weight**	**Energy**
$(n,x\gamma)$	6748119	4.55594	4.72562	6733336	4.54900	4.71720	0.22	0.15	0.18
Compton	10701902		2.05220	10984860		2.05072	2.58		0.07
pair prod	201878	0.13729	0.39470	200888	0.13658	0.39256	0.49	0.52	0.54
e^+-annihil	403756	0.27457	0.14031	401776	0.27316	0.13959	0.49	0.52	0.51
capture'	5601407	3.96544	1.68789	5592790	3.95956	1.68460	0.15	0.15	0.20
leakage	1348590	0.72780	0.73262	1341433	0.72600	0.72741	0.53	0.25	0.72

4.2. Flux Tallies

Another example of basic testing we utilized was to verify the MCATK track-length fluxes compared to the MCNP6 track-length fluxes. The flux calculation starts with a bare sphere of Uranium-235 that has a radius = 8.4707 cm and a density = 18.7 g/cm^3 and uses a mono-energetic (1.0 MeV) neutron point source located at the center of the sphere with 1 million Monte Carlo particles. The flux tallies were on 25 equal radially spaced spherical shells using two energy bins that have edges for neutrons of $(1x10^{-11},\ 0.5,\ 20.0)\ MeV$ and for photons of $(1x10^{-11},\ 1.0,\ 20.0)\ MeV$. The time-dependent flux calculation is time integrated from 0 to 1 *shake*. Both neutron and photon fluxes were tallied from this coupled n-γ calculation. Tables 3 and 4 present the track-length flux comparisons for neutrons and photons, respectively. The actual scalar fluxes from MCNP6 are presented along with the MCATK absolute relative difference to the MCNP6 results.

For the flux tallies comparison, some MCNP6 physics was turned off for consistency with MCATK: Compton Doppler broadening, fluorescence, thick-target Bremsstrahung approximation, and unresolved resonance treatments.

For the neutron flux, MCATK and MCNP match very well to less than 0.5 percent. Notice that the relative difference between the two codes grows slightly with increased radius. Similarly, for the photon flux, MCATK and MCNP are in good agreement with to less than 1.6 percent and, again, the relative difference increases with the increase in radius. We are not sure about this consistent increase in flux with radius at this time.

Table 3: Comparison of MCATK and MCNP6 *neutron* flux $[neutron/cm^2/sh]$ from a time-dependent calculation of a Uranium sphere. Relative difference calculations were performed $(MCNP - MCATK)/MCNP$.

	MCNP Flux			MCATK Flux Relative Diff.		
Cell	**< 0.5 MeV**	**> 0.5 MeV**	**Total**	**< 0.5 MeV**	**> 0.5 MeV**	**Total**
1	5.13e-02	2.10e+00	2.15e+00	1.69e-03	-4.56e-04	-4.07e-04
2	2.49e-02	3.48e-01	3.73e-01	-3.86e-03	-1.03e-03	-1.47e-03
3	1.64e-02	1.48e-01	1.65e-01	-3.04e-03	-3.67e-04	-6.33e-03
4	1.21e-02	8.71e-02	9.92e-02	-2.71e-03	-4.69e-04	-7.42e-04
5	9.41e-03	5.92e-02	6.86e-02	-1.80e-03	1.80e-05	-2.33e-04
6	7.55e-03	4.39e-02	5.14e-02	1.70e-03	-4.70e-04	-1.50e-04
7	6.18e-03	3.41e-02	4.03e-02	1.43e-04	-6.27e-04	5.09e-04
8	5.10e-03	2.75e-02	3.26e-02	5.30e-05	-5.07e-04	-4.21e-04
9	4.22e-03	2.26e-02	2.68e-02	3.13e-04	-4.95e-04	-3.67e-04
10	3.52e-03	1.89e-02	2.24e-02	1.52e-03	-8.03e-04	-4.40e-04
.....	.....	.....	.....	.....	.....	.....
21	4.19e-04	3.39e-03	3.80e-03	1.88e-03	4.76e-04	6.30e-04
22	3.32e-04	2.85e-03	3.19e-03	3.85e-03	1.29e-03	1.55e-03
23	2.59e-04	2.38e-03	2.64e-03	4.87e-03	1.15e-03	1.51e-03
24	1.94e-04	1.95e-03	2.14e-03	3.98e-03	1.13e-03	1.39e-03
25	1.31e-04	1.53e-03	1.66e-03	2.32e-03	2.00e-03	2.02e-03

Table 4: Comparison of MCATK and MCNP6 *photon* flux $[photons/cm^2/sh]$ from a time-dependent calculation of a Uranium sphere. Relative difference calculations were performed $(MCNP - MCATK)/MCNP$.

	MCNP Flux			MCATK Flux Relative Diff.		
Cell	**< 1.0 MeV**	**> 1.0 MeV**	**Total**	**< 1.0 MeV**	**> 1.0 MeV**	**Total**
1	1.76e-01	1.12e-01	2.88e-01	2.94e-03	5.74e-03	4.03e-03
2	5.67e-02	4.49e-02	1.02e-01	3.73e-03	6.52e-03	4.97e-03
3	2.92e-02	2.61e-02	5.53e-02	6.44e-03	6.72e-03	6.57e-03
4	1.86e-02	1.78e-02	3.64e-02	6.88e-03	9.43e-03	8.12e-03
5	1.33e-02	1.32e-02	2.65e-02	9.59e-03	8.71e-03	9.15e-03
6	1.01e-02	1.03e-02	2.04e-02	1.12e-02	8.19e-03	9.69e-03
7	7.98e-03	8.30e-02	1.63e-02	1.12e-02	9.98e-03	1.06e-02
8	6.49e-03	6.81e-03	1.33e-02	1.09e-02	1.20e-02	1.15e-02
9	5.37e-03	5.70e-03	1.11e-02	1.33e-02	1.11e-02	1.21e-02
10	4.51e-03	4.81e-03	9.32e-03	1.37e-02	1.28e-02	1.33e-02
.....	.....	.....	.....	.....	.....	.....
21	7.95e-04	8.59e-04	1.65e-03	1.05e-02	1.54e-02	1.30e-02
22	6.64e-04	7.16e-04	1.38e-03	1.17e-02	1.53e-02	1.35e-02
23	5.44e-04	5.86e-04	1.13e-03	1.04e-02	1.34e-02	1.20e-02
24	4.29e-04	4.60e-04	8.88e-04	1.13e-02	1.61e-02	1.38e-02
25	2.94e-04	3.26e-04	6.19e-04	1.23e-02	1.67e-02	1.46e-02

5. Summary

We have presented and described the present state of Monte Carlo continuous energy photon transport in MCATK. The basics of the four photoatomic processes (coherent scattering, incoherent scattering, pair-production, and photoelectric effect) have introduced and described. A fifth primary photon process (photodisintegration) was ignored at this time due to the incident photon high-energy thresholds (greater than 8 MeV) and the smaller interaction probabilities compared to some of the other photoatomic processes.

In this document, we describe how we implemented the sampling of the four photoatomic processes, especially coherent and incoherent scattering. This was followed up with some basic unit test comparisions to analytic and MCNP results. We, also, have documented two basic integrated tests (for collision and flux tallies) we used to compare to MCNP. Also included is a brief summary of photon production from neutron interactions, which provides the MCATK library with the ability to do Monte Carlo coupled neutron-photon transport.

Presently, MCATK does not model Bremsstrahlung or fluorescence produced. To be clear, MCATK completely ignores the electrons (including any electron energy deposition) at this time. The MCATK team hopes to include feature improvements in these areas in near future.

6. Acknowledgements

We thank Miss Emily Adams for providing the drawings for the basic photon interactions in Figs. 2, 8, 19, 20. The authors would like to thank one of their co-authors, Grady Hughes, for sharing his time and expert knowledge of the domain space.

References

Adams, T., Nolen, S., Sweezy, J., Zukaitis, A., Campbell, J., Goorley, T., Greene, S., Aulwes, R., 2015. "Monte Carlo Application ToolKit (MCATK)". Annals of Nuclear Energy 82 (0), 41–47. URL http://www.sciencedirect.com/science/article/pii/S0306454914004472

Blomquist, R. N., Gelbard, E. M., 1983. "An Assessment of Existing Klein-Nishina Monte Carlo Sampling Methods". Nuclear Science and Engineering 83, 380–384.

Bohm, D., 1958. Quantum Theory. Prentice-Hall, Inc., Englewood Cliffs, New Jersey, US.

Brown, L. M., 2002. "The Compton Effect as One Path to QED". Studies in History and Philosophy of Modern Physics 33, 211–249.

Carter, L. L., Cashwell, E. D., 1977. "Particle-Transport Simulation with the Monte Carlo Method". Tech. Rep. TID-26607, ERDA Technical Information Center, Oak Ridge, Tennessee, US.

Charlton, M., Humberston, J. W., 2001. Positron Physics. Cambridge University Press, Cambridge, UK.

Compton, A. H., 1923. "A Quantum Theory of the Scattering of X-rays by Light Elements". Physical Review 21, 483.

Debye, P., 1923. "Zerstreuung von Röntgenstrahlen und Quantentheorie". Zeitschrift fr Physik 24, 161–166.

Debye, P., 1954. "X-Ray Scattering and Quantum Theory". In: The Collected Papers of Peter J.W. Debye. Interscience Publishers, Inc., New York, New York, US, pp. 80–88.

Einstein, A., 1905. "Über einen die Erzeugung und Verwandlung des Lichtes betreffenden heuristischen Gesichtspunkt". Annalen der Physik 322, 132–148.

Einstein, A., 1967. "On a Heuristic Point of View about the Creation and Conversion of Light". In: Haar, D. T. (Ed.), The Old Quantum Theory. Pergamon Press, Oxford, UK, Ch. 3, pp. 91–107.

Emigh, C. R., 1970. "Thick Target Bremsstrahlung Theory". Tech. Rep. LA-4097-MS, Los Alamos National Laboratory, Los Alamos, New Mexico, US.

Evans, R. D., 1958. "Compton Effect". In: Flugge, S. (Ed.), Encyclopedia of Physics: Corpuscles and Radiation in Matter II. Vol. XXXIV. Springer-Verlag, Berlin, DE, pp. 218–298.

Evans, R. D., 1982. The Atomic Nucleus. Robert E. Krieger Publishing Company, Malabar, Florida, US, (Reprint Edition of 14th Printing 1972).

Fernández, J., Hubbell, J., Hanson, A., Spencer, L., 1993. "Polarization Effects on Multiple Scattering Gamma Transport". Radiation Physics and Chemistry 41 (4), 579–630. URL http://www.sciencedirect.com/science/article/pii/0969806X9390316M

Goorley, T., James, M., Booth, T., Brown, F., Bull, J., Cox, L. J., Durkee, J., Elson, J., Fensin, M., Forster, R. A., Hendricks, J., Hughes, H. G., Johns, R., Kiedrowski, B., Martz, R., Mashnik, S., McKinney, G., Pelowitz, D., Prael, R., Sweezy, J., Waters, L., Wilcox, T., Zukaitis, T., 2012. "Initial MCNP6 Release Overview". Nuclear Technology 180, 298–315.

Horner, W. G., 1819. "A New Method of Solving Numerical Equations of All Orders, by Continuous Approximation". Philosophical Transactions of the Royal Society of London 109, 308–335. URL http://www.jstor.org/stable/107508

Hubbell, J. H., 1997. "Summary of Existing Information on the Incoherent Scattering of Photons, Particularly on the Validity of the use of The Incoherent Scattering Function". Radiation Physics and Chemistry 50, 113–124.

Hubbell, J. H., 1999. "Review of Photon Interaction Cross Section Data in the Medical and Biological Context". Physics in Medicine and Biology 44 (13), R1–R22.

Hubbell, J. H., 2006a. "Electron-Positron Pair Production by Photons". Radiation Physics and Chemistry 75 (6), 614–623.

Hubbell, J. H., 2006b. "Review and History of Photon Cross Section Calculations". Physics in Medicine and Biology 51 (13), R245–R262.

Hughes, H. G., 2013a. "Enhanced Electon-Photon Transport in MCNP6". Tech. Rep. LA-UR-13-27632, Los Alamos National Laboratory, Los Alamos, New Mexico, US.

Hughes, H. G., 2013b. "An Electron/Photon/Relaxation Data Library for MCNP6". Tech. Rep. LA-UR-13-27377, Los Alamos National Laboratory, Los Alamos, New Mexico, US.

Hughes, H. G., 2013c. "Enhanced Electon-Photon Transport in MCNP6". Tech. Rep. LA-UR-13-27378, Los Alamos National Laboratory, Los Alamos, New Mexico, US.

Jackson, J. D., 1975. Classical Electrodynamics, 2nd Edition. John Wiley and Sons, Inc., New York, New York, US.

Kahn, H., 1956. "Applications of Monte Carlo". Tech. Rep. RM-1237-AEC, The RAND Corporation.

Klein, O., Nishina, Y., 1929. "Über die Streuung von Strahlung durch freie Elektronen nach der neuen relativistischen Quantendynamik von Dirac". Zeitschrift fr Physik 52, 853–868.

Klein, O., Nishina, Y., 1994. "On the Scattering of Radiation by Free Electrons According to Dirac's New Relativistic Quantum Dynamics". In: Ekspong, G. (Ed.), The Oskar Klein Memorial Lectures. Vol. 2. World Scientific Publishing Company, Singapore, pp. 113–139.

Knuth, D., 1998. The Art of Computer Programming, Volume Two, Seminumerical Algorithms, 3rd Edition. Addison-Wesley, Reading, Massachusetts, US.

Koblinger, R., 1975. "Direct Sampling from the Klein-Nishina Distribution for Photon Energies Above 1.4 MeV". Nuclear Science and Engineering 56, 218–219.

Lux, E., Koblinger, L., 1991. Monte Carlo Particle Transport Methods: Neutron and Photon Calculations. CRC Press, Boca Raton, Florida, US.

MacFarlane, R. E., Muir, D., 1997. "The NJOY Nuclear Data Processing System Version 9.1". Tech. Rep. LA-12740-M, Los Alamos National Labratory, Los Alamos, New Mexico, US.

Millikan, R. A., 1916. "A Direct Photoelectric Determination of Planck's 'h'". Physical Review 7, 355.

Pratt, R. H., 2014. "Photon Absorption and Photon Scattering–What We Do Not Know and Why it Matters". Radiation Physics and Chemistry 95, 4–13.

Ramella-Roman, J. C., Prahl, S. A., Jacques, S. L., Jun 2005. "Three Monte Carlo Programs of Polarized Light Transport into Scattering Media: Part I". Optical Express 13 (12), 4420–4438. URL http://www.opticsexpress.org/abstract.cfm?URI=oe-13-12-4420

Roy, S. C., Kissel, L., Pratt, R. H., 1999. "Elastic Scattering of Photons". Radiation Physics and Chemistry 56, 3–26.

Roy, S. C., Pratt, R. H., Kissel, L., 1993. "Rayleigh Scattering by Energy Photons: Development of Theory and Current Status". Radiation Physics and Chemistry 41 (4/5), 725–738.

Strutt, J. W., 1871a. "On the Light From the Sky, Its Polarization and Colour". Philosophical Magazine 41, 107.

Strutt, J. W., 1871b. "On the Light From the Sky, Its Polarization and Colour". Philosophical Magazine 41, 274.

Sweezy, J., 2016. "Photon Next-Event Estimators Implementation in MCATK". Tech. Rep. LA-UR-16-xxxx, Los Alamos National Laboratory, Los Alamos, New Mexico, US.

Sweezy, J., Nolen, S., Adams, T., Trahan, T., Pritchett-Sheats, L., 2015. "Monte Carlo Application ToolKit (MCATK): Advances for 2015". Tech. Rep. LA-UR-15-20016, Los Alamos National Laboratory, Los Alamos, New Mexico, US, ANS MC2015 - Joint International Conference on Mathematics and Computation (M&C), Supercomputing in Nuclear Applications (SNA) and the Monte Carlo (MC) Method, 2015-04-19 (Nashville, Tennessee, US).

Thomson, J. J., 1903. Conduction of Electricity through Gases. Cambridge University Press, Cambridge, UK.

Turner, J. R., 1992. Atoms, Radiation, and Radiation Protection. McGraw-Hill, New York, New York, US.

Veigele, W. J., Tracy, P. T., Henry, E. M., 1966. "Compton Effect and Electron Binding". American Journal of Physics 34, 1116–1121.

Wolfram Research, Inc., 2015. "Mathematica 10.1". URL https://www.wolfram.com

X-5 Monte Carlo Team, 2003 Revised 2/1/2008. “MCNP - A General Monte Carlo N-Particle Transport Code, Version 5, Volume I: Overview and Theory”. Tech. Rep. LA-UR-03-1987, Los Alamos National Laboratory, Los Alamos, NM, US.
URL https://laws.lanl.gov/vhosts/mcnp.lanl.gov/pdf_files/la-ur-03-1987.pdf

Appendix A. Direct Probability of Scattering Distributions

For this section, we draw heavily from the "Photon Next-Event Estimators Implementation in MCATK" report by Sweezy (2016). Both coherent and incoherent scattering events result in a scattered photon. For coherent and incoherent scattering we can *directly* calculate (not sample) the probability of scattering (PSC) in a given direction, $\mu = \cos\theta$. This probability often is expressed as $p(Z,R,E \rightarrow E',\mu)$ with resulting energy E', for reaction R of isotope Z given an incident energy E.

For coherent scattering, the probability of scattering into a given angle is given by the ratio of the differential coherent cross section to the total coherent cross section by

$$p_{coh}(Z,E,\mu) = \frac{\sigma_{coh}(Z,E,\mu)}{\sigma_{coh}(Z,E)}\,, \tag{A.1}$$

where $\sigma_{coh}(Z,E,\mu)$ is the differential coherent cross section at angle μ and $\sigma_{coh}(Z,E)$ is the total coherent reaction cross section

$$\sigma_{coh}(Z,E) = \int_{-1}^{1} \sigma_{coh}(Z,E,\mu)d\mu\,. \tag{A.2}$$

The differential coherent cross section is calculated from the modified differential Thomson cross section (see Eq. (3))

$$\sigma_{coh}(Z,E,\mu) = C^2(Z,E,\mu)\; T(\mu)\,, \tag{A.3}$$

where $C^2(Z,E,\mu)$ is the square of the coherent form factor, and $T(\mu)$ is the differential Thomson cross section (see Eq. (1)). The outgoing energy for coherent scattering is equal to the incoming energy

$$E'_{coh} = E\,. \tag{A.4}$$

For incoherent scattering, the probability of scattering into a given angle is given by the ratio of the differential incoherent cross section to the total incoherent cross section by

$$p_{incoh}(Z,E \rightarrow E',\mu) = \frac{\sigma_{incoh}(Z,E \rightarrow E',\mu)}{\sigma_{incoh}(Z,E)}\,, \tag{A.5}$$

where $\sigma_{incoh}(Z,E,\mu)$ is the differential incoherent cross section at angle μ and $\sigma_{incoh}(Z,E)$ is the total incoherent reaction cross section

$$\sigma_{incoh}(Z,E) = \int_{-1}^{1} \sigma_{incoh}(Z,E \rightarrow E',\mu)d\mu\,. \tag{A.6}$$

The differential incoherent cross section is calculated from a modification of the differential Klein-Nishina cross section (see Eq. (11))

$$\sigma_{incoh}(Z,E \rightarrow E',\mu) = I(Z,E,\mu)\; K(E,\mu)\,, \tag{A.7}$$

where $I(Z,E,\mu)$ is the incoherent form factor, and $K(E,\mu)$ is the differential Klein-Nishina cross section (see Eq. (7)). The outgoing energy is based on the Compton energy collision formula (see Eq. (5)).